STUDY THE CONSERVATION DEGREE IN WOOD STRUCTURES USING TDR AND GPR TECHNIQUES

De Giorgi[1] L., Barbolla[1] D. F., Comisi[2] F., Torre[2] C., Leucci[1*] G.

[1]*Institute of Heritage Sciences, National Research Council, 73100 Lecce*
[2]*University of Catania, 95124 Catania*
[*]*corresponding author, giovanni.leucci@cnr.it*

Abstract

The condition of the wood structure and its components should be carefully recorded before considering any action. The diagnosis of wood structures in heritage should precede any intervention. Is important to know preliminarily the construction and structural system, the decay condition and the causes. Furthermore, damage or structural failure should be considered. The diagnosis must be based principally on measurements of physical parameters using non-destructive testing, and if necessary on laboratory testing. Water is one of the principal causes of wood decay. In this study Ground-penetrating radar (GPR) and time domain reflectometry (TDR) was used to estimate the dielectric permittivity and successively the volumetric water content of several types of wood. An empirical relationship was found between the dielectric constant and volumetric water content. Results were applied to two case study: the Cathedral of Foggia and the castle of Carosino.

Keywords: TDR, GPR, wood structures

Introduction

The volumetric water content in a wood structures is related to their conservation state. Changes in wood volumetric water content lead to changes of the physical and mechanical properties such as for example strength and stiffness properties. The existence of high volumetric water content can initiate decay or growth of fungi. Therefore the estimation of the volumetric water content and the subsequent initiation of potentially necessary measures are therefore essential tasks during the planning, execution and maintenance of the wood structures expecially in the heritage field. The in-situ monitoring of moisture content of structural timber elements has recently received considerable interest and growth.

To determine wood volumetric water content two methods can be taken into consideration: that of direct measurements (EN 13183-1, 2002), and that of indirect measurements (Kollmann and Coté,

1968; Niemz, 2003; EN 13183-3, 2005).

In direct measurements, the moisture content is determined by oven-drying or water extraction, whereby both are destructive methods. Indirect measurement methods use physical properties of wood which are correlated to the wood moisture content. The indirect measurements can be performed using geophysical metods. Electrical resistivity tomography (ERT) using a ring array of needle electrodes was applied by Al Hagrey (2006) to image the internal electrical structures of the trunks of living standing trees and trunk disks. Baranski et al. 2021 used ERT method to determine the influence of the impregnation process of pine wood (Pinus sylvestris) samples on the electrical resistance changes and the moisture-content. They found an empirical relationship valid only for the Pinus sylvestris.

Mai et al. presents some laboratory measurements in the aim of studying the sensitivity of EM waves propagation properties to moisture variation and fibers direction in wood material. Spruce and Pine wood samples were considerated. Also in this case the correlation between the dielectric constant and moisture content was useful only for the two type of woods.

Furthermore the electromagnetic characteristics of the wood are of great interest within GPR prospecting related to the study of the conservation state of the wooden structures. In particular, these characteristics, if correctly retrieved, allow not only a correct time-depth conversion (Daniels, 2004) but also a correct focusing of the buried targets (such as voids, knots, etc.) through migration or, more in general, an inversion algorithm (Leucci et al., 2007).

Moreover, depending on the applications, the characteristics of the medium can be crucial in themselves and not only in relationship to the reconstruction and interpretation of the targets. This can happen, e.g. when the "final" quantity of interest is the water content of the wood (Topp et al., 1980). In general, the dielectric permittivity and the electrical conductivity of the embedding medium depend in a meaningful way, but also in a complicated and often unknown way, on the chemical, physical and mineralogical properties mixture composing the wood at hand. This makes it quite hard to get a reliable a-priori knowledge of them. In particular, some experimental values or semi-empirical laws are available (Daniels, 2004; Jol, 2009); nevertheless, they should be considered reference-average quantities, which are helpful to test the likelihood of a measure in the field but should not replace it.

In particular, the measure of the dielectric permittivity of the wood can be performed from the same GPR data (Lambot et al., 2004; Soldovieri et al., 2008), classically using the shape of the diffraction

curves. Alternatively, the dielectric permittivity can be evaluated through the time domain reflectometry (TDR) technique (Cataldo et al., 2011).

In this paper, a new comparative experimental evaluation of the dielectric permittivity of some wood samples (fir, beech, maple, chestnut, cherry, ash and pine) is proposed. Results show an agreement between the diffraction curve method analysis and the TDR measurements. An empirical relationship was found between dielectric constant and volumetric water content in the exsaminated wood structures. Results were applied to two case studies related to the analysis of the conservation state of the wood beams first one of the Cathedral of Foggia and secondo ne the castle of Carosino (Apulia region, south Italy).

Time Domain Reflectometry measurements

The experimental setup for TDR measurements included a TDR unit (Campbell Scientific TDR100), a non-invasive probe and a 1.0 m-long 50 Ω-matched coaxial cable that connected the probe to the TDR unit (Fig. 1).

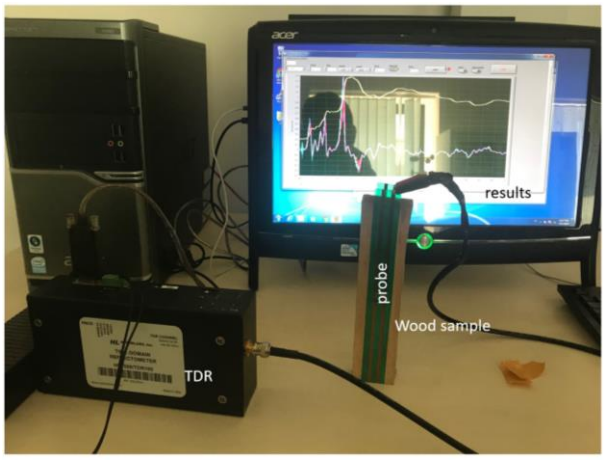

Fig. 1: The TDR experimental set up

The TDR100 generates a step-pulse signal with a rise-time of 200 ps, which corresponds to a frequency bandwidth of approximately 1.7 GHz.

The wood samples have been dehydrated at 105 Celsius for 24 hours. In particular, drying wood prevents inhomogeneity due to possible gradients of moisture content. Moreover, dehydration also reduces the dependence of the permittivity on potential gradients of density. Successively the samples were immersed in water and saturated. The relative dielectric permittivity of the prepared sample was determined through the well-known TDR method (Robinson et al., 2003). In TDR measurement, the

step-pulse signal generated by the TDR unit propagates along the probe inserted in the material under test; the reflected signal is acquired by the same TDR unit and displayed in terms of reflection coefficient, a function of the apparent distance in the air.

As detailed in ref. (Cataldo et al., 2009), for low-loss and low-dispersive materials, the relative dielectric permittivity can be evaluated through the following equation:

$$\varepsilon \cong \left(\frac{L_{app}}{L_{phys}} \right)^2 \qquad (1)$$

where Lapp is the apparent distance of the probe inserted in the sample under test (Lapp is calculated directly from the TDR waveform), and Lphys is the probe's physical (actual) length (Fig. 2).

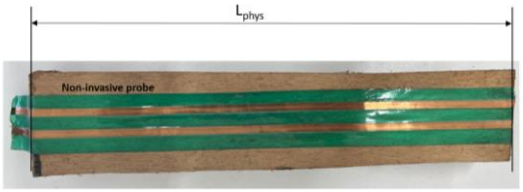

Fig. 2: The non-invasive probe

According to Baletrieri et al., (2012), the accurate value of Lphys was evaluated through preliminary TDR measurements performed in air and distilled water (this was necessary because a tiny portion of the sensing element is contained in a Teflon cap, and this portion must be correctly subtracted to obtain the actual value of Lphys).

For the case considered herein, reference TDR measurements were performed using the non-invasive three-rod probe. For each acquisition, the instrumental averaging number was 128. The number of sample points for each waveform was 2,048.

For example, Fig. 3 shows one of the acquired TDR waveforms and the corresponding first derivative curve. The derivative facilitates the evaluation of Lapp; in fact, the first peak of the derivative (occurring approximately at 62 mm) corresponds to the beginning of the probe, whereas the second one (occurring around 55 mm) corresponds to the open-ended probe termination.

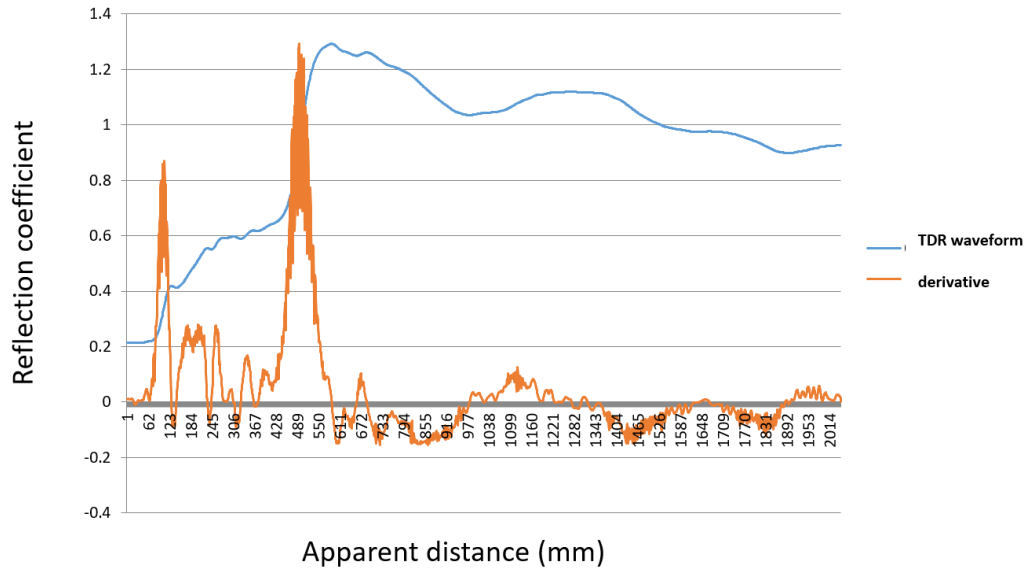

Fig. 3. The location of geophysical surveys TDR waveform (blue curve) and corresponding first derivative (orange curve) obtained for the wet maple

The relative dielectric permittivity of the sand, calculated through equation (1) and averaged over the four measurement points, is 3.2 (evaluated with a corresponding expanded uncertainty of 3%).

The Diffraction Curve Method

The diffraction curve method is based on the matching between the data and a model describing the two-way time of the GPR signal. This model provides a curve while considering the movement of the antenna over the target. In particular, given an electrically small target (in our case the bar with the small cross section in terms of the probing wavelength) at the abscissa x_o, if the offset between the transmitting and receiving antennas is neglected, with reference to fig. 4, the model for the diffraction curve is given by

$$t = \frac{2}{c}\sqrt{(x - x_o)^2 + \left(\frac{ct_o}{2}\right)^2} \qquad (1)$$

where c is the propagation velocity in the soil, linked to the relative permittivity ε_{sr} by the well-known relationship $c = \frac{c_o}{\sqrt{\varepsilon_{sr}}}$, and t_o is the minimum recorded time, gathered when the source-

observation point flies just over the target, so that $x = x_o$.

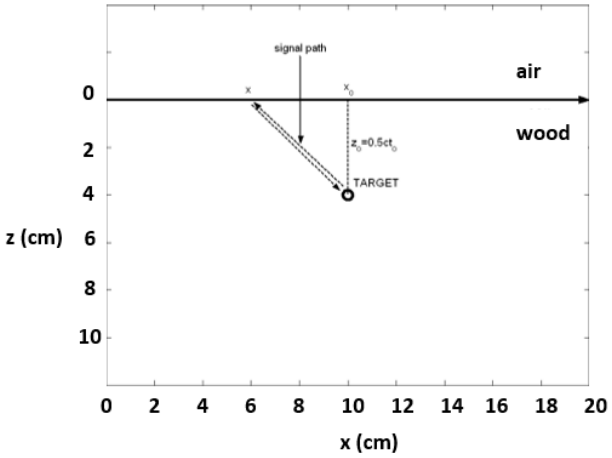

Fig. 4: Schematic of the round trip time vs. the source-observation point for common (null) offset GPR data.

As well known, we can recognise that the diffraction curve is in this case a branch of hyperbola. Conversely, if the offset Δ between the antennas is accounted for, after some manipulation, eq. 1 can be re-written as follows:

$$t = \frac{1}{c}\sqrt{\left(x - x_o - \frac{\Delta}{2}\right)^2 + \left(\frac{ct_o}{2}\right)^2 - \left(\frac{\Delta}{2}\right)^2} + \\ + \frac{1}{c}\sqrt{\left(x - x_o + \frac{\Delta}{2}\right)^2 + \left(\frac{ct_o}{2}\right)^2 - \left(\frac{\Delta}{2}\right)^2} \qquad (2)$$

where Δ is specifically the offset between source and observation point, and x indicates the midpoint between source and observation locations. In this work, eq. 2 was considered, accounting for the offset between the actual gaps of the 2 GHz antennas, equal to 5 cm. Although the effect of this offset is not strong, it rigorously makes the diffraction curve not to be a hyperbola any longer.

In particular, a range of diffraction curves ranging from the trial value $\varepsilon=2$ (top curve in fig. 5) to the trial value $\varepsilon=4$ (lowest curve in fig. 5) was considered. The curves have been ranged with a step $\Delta\varepsilon=0.2$; however, for graphical reasons in fig. 5, only the extreme curves and the best matching curve (which has been heuristically seen to correspond to $\varepsilon=3$), are reported. As aforementioned, the best

matching has been heuristic, i.e. worked out from the visual correspondence between the field scattered by the metallic bar and the superposed diffraction curve.

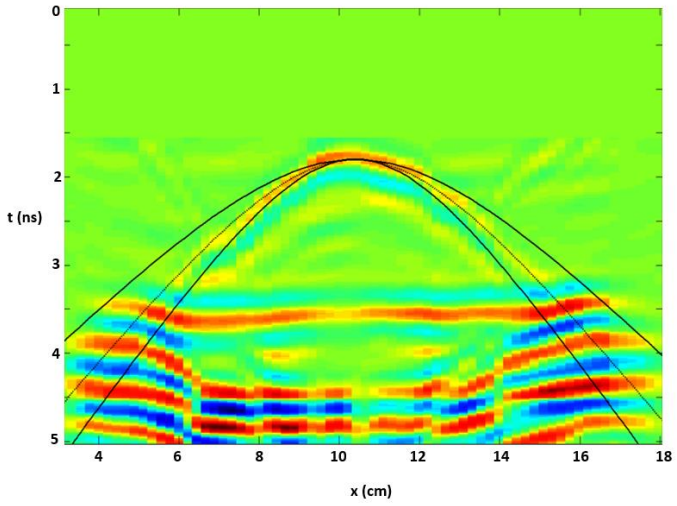

Fig. 5. The model with diffraction curves for ε=2 (upper solid line), ε=3 (central dashed line) and ε=4 (lower solid line).

The measurements were performed with an IDS Ris Hi-mode system equipped with the antenna at a nominal central frequency of 2 GHz. The choice of this antenna is related to the high vertical (VR) and horizontal (HR) resolution. The below relationships allow to estimate the VR and HR (Leucci, 2019, Giannino and Leucci, 2021).

$VR= T_{pulse} \cdot c / 2 (\varepsilon)^{1/2}$

Where T_{pulse} is the transmitted pulse duration, this can be calculated by taking the inversion of the fundamental or center frequency, c is the velocity of light in vacuum, ε is the relative dielectric permittivity of the media.

$HR= [c/ 4 \cdot f \cdot (\varepsilon)^{1/2}] + [D / (\varepsilon+1)^{1/2}]$

c is the velocity of light in vacuum, f is the center frequency of the antenna, ε is the relative dielectric permittivity, D is the depth of the object.

Considering a dielectric constant of 3,2 and a depth of the metal rod of about 0.05m, VR and HR are 0.05m and 0.045m respectively. The frequency of 2GHz was a quite good choice because the thickness of the samples varies from 0.1m to 0.12 m while the diameter of the iron bar is 0.045 m.

Each B-scan has a time window of 32 ns, discretized using 2048 samples. The trace interval was 0.002m. When moving the antenna on the wood, extreme care was taken to pull the antenna at a constant velocity. The repetition of the scan along the same line three times has allowed a test about the uniformity of the antenna movement velocity. For GPR measurements, the experimental setup was a wooden sample on a metal rod (Fig. 6). This allows us to analyze the data using the diffraction curve method.

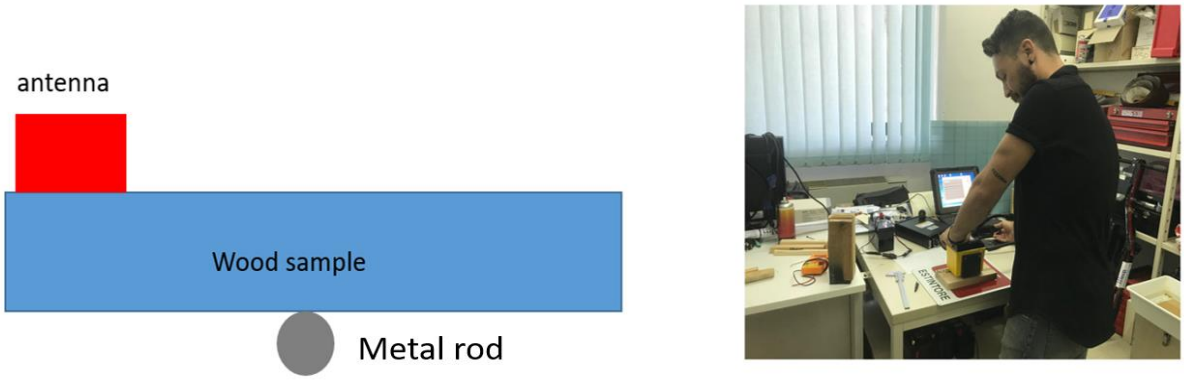

Fig. 6. GPR experimental setup

The dielectric permittivity value has been assessed also by the focussing procedure presented in Lambot et al. (2004). The approach is based on the determination of the dielectric permittivity of the medium as the one that, when introduced in a Born model based inversion model, is able to produce "the most focussed" image of a target whose cross-section is small in terms of the probing wavelength (smaller than the resolution limits).

Thus, the procedure can be summarised as follows. For each trial value of the dielectric permittivity of the medium, a key factor in the definition of the Born inverse model, we performed the Truncated Singular Value Decomposition (TSVD) regularised inversion of the targets in terms of the modulus of the contrast function (Lambot et al., 2004). The value of the dielectric permittivity of the medium is estimated as the one producing the most "focussed" reconstruction of the marker (in the considered case, the metallic bar). The question arises about how to quantify the "focussing effect" and in the previous studies we have considered two parameters, namely the maximum of the modulus of the contrast function and the minimum extent of the spot representing the target in the reconstructed

image (Soldovieri et al., 2008). A detailed description of the two indexes and of the performances of the estimation procedures related to their choice are given in Soldovieri et al., (2008), Soldovieri et al., (2009).

Let us turn now to consider the results for the case discussed herein.

The microwave tomographic approach exploited to achieve images of the targets was implemented with the following parameters: 35 uniformly spaced frequencies within the work band 1-3 GHz; 43 spatial points with step 0.022 m; an investigation domain with 0.9 extent along the antenna movement direction and raging from 0.05 m to 0.5 m in depth. A multibistatic configuration has been considered, with fixed offset of 5 cm between the source and observation point. The inversion approach exploited a TSVD regularization scheme with threshold for the singular values at -20 dB.

Fig. 7 depicts the modulus of the reconstructed contrast function at the variance of the relative dielectric permittivity inserted in the Born model in three cases, in order to show the capabilities of the inversion algorithm.

Instead, in fig. 8, the maximum value of the retrieved contrast modulus at the variance of the trial permittivity is depicted. The two curves are relative to two different choices for the zero-time the B-scan, represented in fig. 9.

This leads to two important considerations. The first is that the estimated relative dielectric permittivity is equal to about 3.1, which is in very good agreement with the diffraction curve based estimation; the second important consideration regards the stability of the estimation procedure with respect to the choice of the time zero.

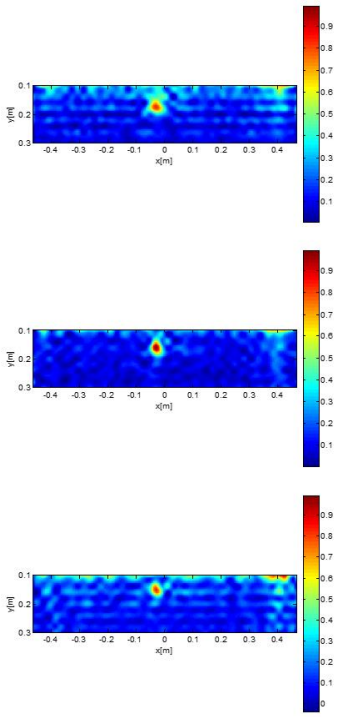

Fig. 7. The focused image on real GPR data for three trial values of the wood permittivity, namely ε=2.6 (upper panel), ε=3.2 (central panel) and ε=4 (lower panel).

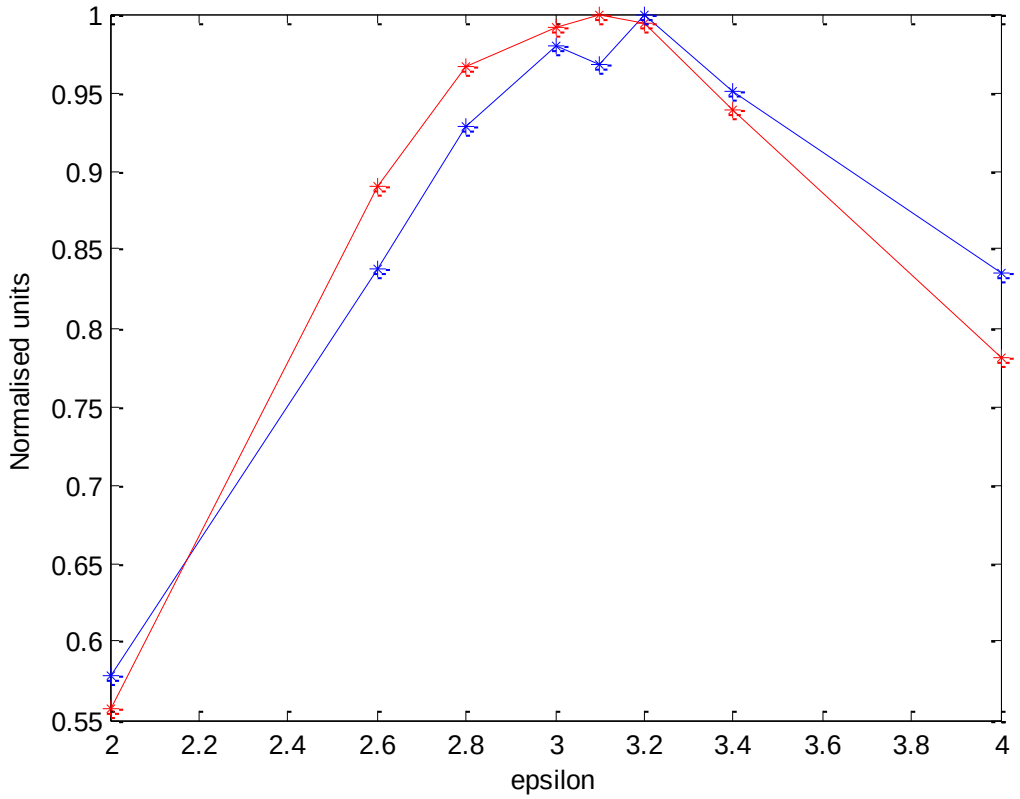

Fig. 8: Maximum contrast modulus vs. the trial dielectric permittivity inserted in the inversion algorithm (The two curves are relative to two different choices for the zero-time)

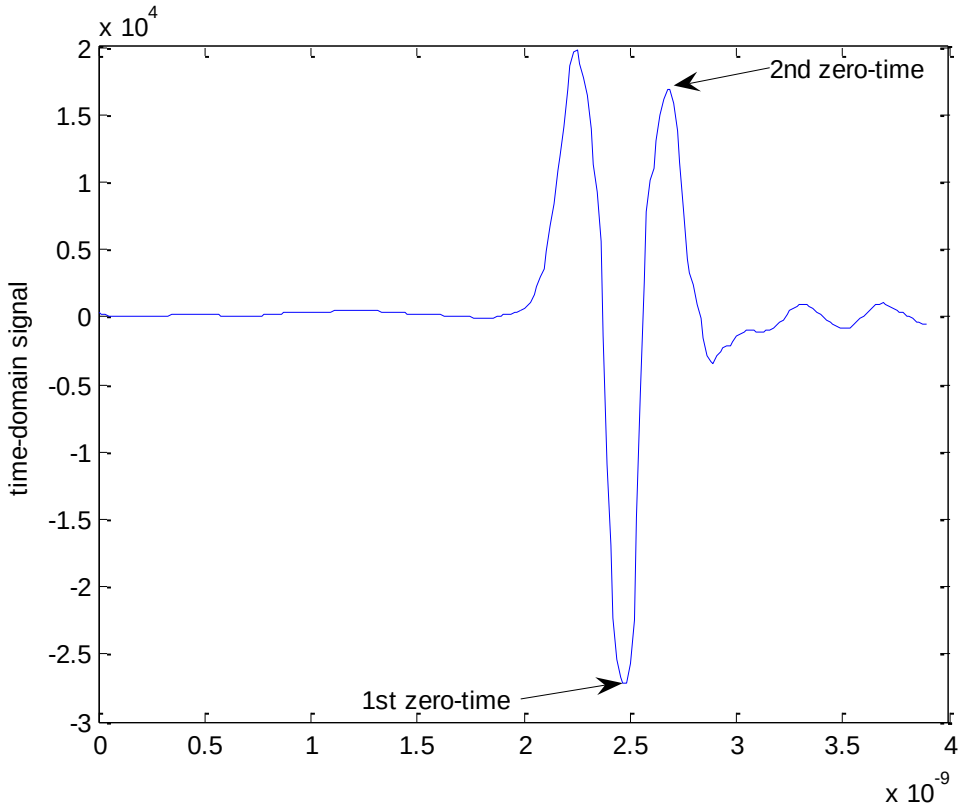

Fig. 9: The two choices adopted for the zero timing

Fig. 10 depicts the behaviour of the other parameter considered in the estimation, i.e., the area of the support of the reconstructed spot. Here, we assume as index the number of pixels of the reconstruction comprised between 0.1 and 1 times the maximum of the contrast function. In Fig. 10 the blue and red line represent the zero time choose (blue line is related to the 1st zero time and red line is related to the 2nd zero time as show in Fig. 9). Also in this case, the estimation returns a value of the dielectric permittivity equal to about 3.1 according to the result of the estimation based on the maximum contrast modulus.

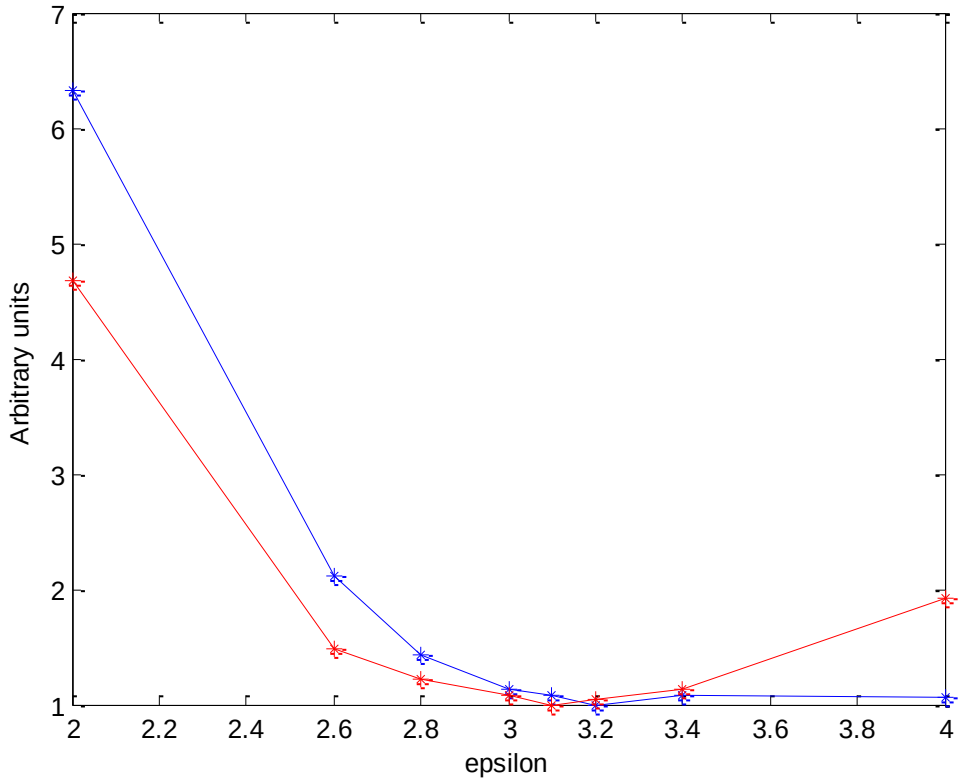

Fig. 10: Area of the support of the retrieved contrast function vs the trial dielectric permittivity inserted in the inversion algorithm (blue line is related to the 1st zero time and red line is related to the 2nd zero time as show in Fig. 9).

Analyzing the results obtained on the different samples with TDR and GPR, the empirical relationship between dielectric constant and volumetric content in water is obtained (Fig. 11).

The dashed line show the function w fitted with the parameters a, b, c and d. in this case the third degree polynomial seems the best choice as we get the correlation coefficient R^2 has a value of 0.837. With other types of fitting the R^2 value was found to be lower. It must clearly be said that, as can be seen from Fig. 11 the quality of the fit appears much poorer for values of dielectric constant greater than 5. This could be due to the microscopic characteristics of the various types of woods examined.

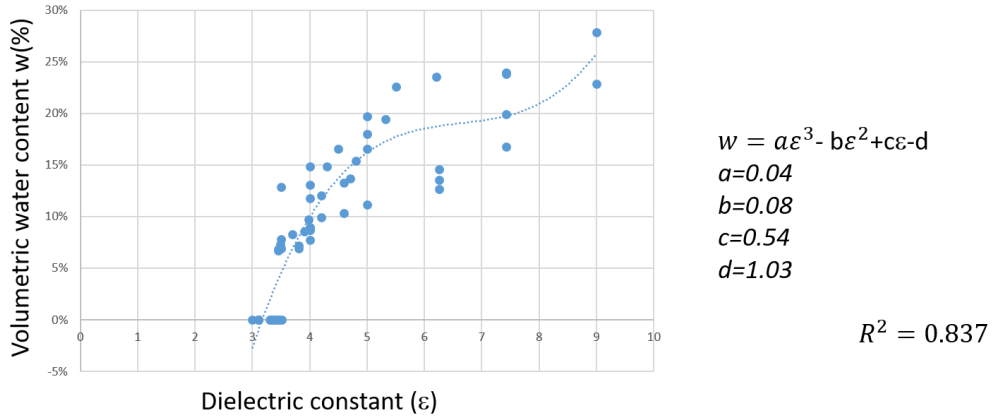

Fig. 11. Relationship between dielectric constant and volumetric water content

The Case Study: The Cathedral of Foggia

The Cathedral of Santa Maria de Fovea, which is directly linked with the patron saint "Madonna dei Sette Veli" (Madonna of the Seven Veils) in Foggia (Fig. 12), of purely Baroque style, was restored after the earthquake of 1731 that almost destroyed the structure. The Cathedral of Foggia is strictly connected to discovering the Icona Vetere religious object, a table that depicts a rare portrait of the Virgin Kiriotissa with seven veils (from which the name of the Madonna with Seven Veils). It was built in 1170 in Romanesque-Apulian style and rebuilt in Baroque style. In 2011, an intervention related to the restoration work of the roof required an in situ investigation campaign aimed at assessing the conservation status of the wooden elements constituting the roofing of the Cathedral. To investigate the quality (compactness, number of nodes, voids, microfractures, etc.) of wooden pieces, ground-penetrating radar (GPR) investigations were performed.

Fig. 12. The Cathedral of Foggia

For this work were used, the GPR IDS-Hi Mod with a 2GHz antenna was used.

All GPR profiles were performed on wooden structures (Fig. 13) and acquired at 1024 samples/track; trace interval of 0.002m; time window of 32ns; the other acquisition parameters were optimized on-site and held constant for each profile.

To eliminate the noise component present in the data, facilitating the interpretation, processing was realized whose phases are listed below: i) background removal; ii) migration using an average EM wave propagation of 0.15m/ns. The presence of various anomalies due to small inhomogeneities, such as nodes and fractures, make possible a rapid and accurate analysis of the velocity of propagation of electromagnetic waves and allowed to obtain the depth of the anomalies. The study of the GPR data (Fig. 14) show that: the radar signal has an excellent penetration and crosses the element investigated for all its thickness; the surface portion of the wooden structures, for a thickness varying from 2 to 5-6 cm, is generally characterized by refl ections of weak amplitude, and this testifi es to a net decrease in the density of the wood, probably related to both the activity of wood-eating insects and chemical attack; this anomaly appears to be more extensive on the extrados of the chains where the infiltration of rainwater, in the presence of significant accumulations of guano, may have generated a corrosive action resulting in breakdown of the cellular elements of the wood; the numerous refl ections in the shape of hyperbole, placed at various depths indicate hardening of woody tissue that, in size and shape, can be related to nodes, single or in groups, their number, sometimes high, determines an average density including between 1.4 and 5.9 nodes per meter, but in some elements of the apse area will reach higher values; reflections with continuous development are generated by sub-horizontal fi ssures almost always oriented in the direction of the grain; their width is generally close to 1 cm; in some of the trusses wood elements B, C, F, G, L of the nave the presence of cavities with dimensions

of the order of 5 cm was recorded, probably due to biological attack. Similar anomalies, presumably correlated to fractures larger than those usually identified, were detected in the trusses L1 (chain, strut right Monaco), L3 (chain), L5 (chain) and L6 (chain). The longitudinal development of these inhomogeneities varies from 15 to 35 cm.

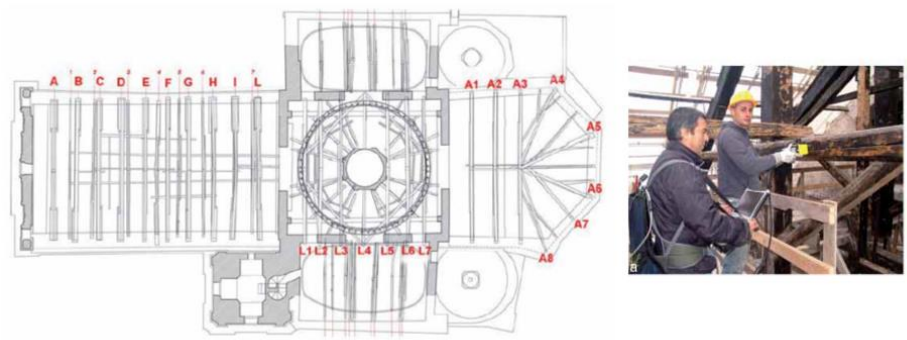

Fig. 13. The roof planimetry: the red letters refer to the position of the wooden structures

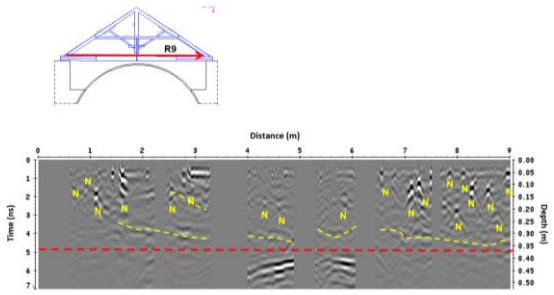

Fig. 14. The processed radar section

Using a point-source reflection (the hyperbolic responses indicated with N) from a buried object to determine the distribution of the 2D electromagnetic (EM) wave velocity. Successively the 2D EM wave velocity and the empirical relationship shown in Fig. 11 allowed us to have a qualitative estimate of the volumetric water content (Fig. 15).

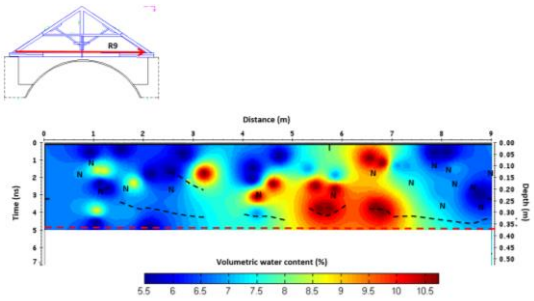

Fig. 15. The distribution of volumetric water content estimed using the 2D EM wave velocity and the relationship shown in Fig. 11.

The 2D distribution of the volumetric water content of the wood varies from about 5% to 10% (Fig. 15). Water content was also measured through a direct mode using a wooden core, and the results agree with those obtained using our relationship.

The Case Study: The Castle of Carosino

The Castle (Fig. 16) was built in the 15th century by the noble Simonetta family, the ducal palace is the heart of the ancient fief of Carosino in the center of the ancient village. After the renovations carried out by the Spanish counts D'Ayala-Valva in the late 19th century, the castle took on the appearance of an ancient Renaissance manor bordered by refined battlements and developed around a square courtyard from which the stairways leading to the first floor where the large halls with barrel or cross vaults follow one another. Since 1895 the building has been owned by the Municipality and is used as a cultural container for the city.

Fig. 16- The Castle of Carosino (Image Landsat/Copernicus Data Sio, NOAA US Navy, NGA, GEBCO Image © 2022 TerraMetrics, Photo Leucci)

To help the restoration work, GPR surveys were carried out on some wooden elements making up the ceiling beams. All GPR profiles were performed on wooden structures (Fig. 17) and acquired used the georadar Ris-Hi-mod with the 2GHz antenna at 1024 samples/track; trace interval of 0.002m;

time window of 32ns; the other acquisition parameters were optimized on-site and held constant for each profile. To eliminate the noise component present in the data, facilitating the interpretation, processing was realized whose phases are listed below: i) background removal; ii) migration using an average EM wave propagation of 0.15m/ns.

The presence of various anomalies due to small inhomogeneities, such as nodes and fractures, make possible a rapid and accurate analysis of the velocity of propagation of electromagnetic waves and allowed to obtain the depth of the anomalies.

Fig. 17- The surveyed wooden structures (photo by Leucci)

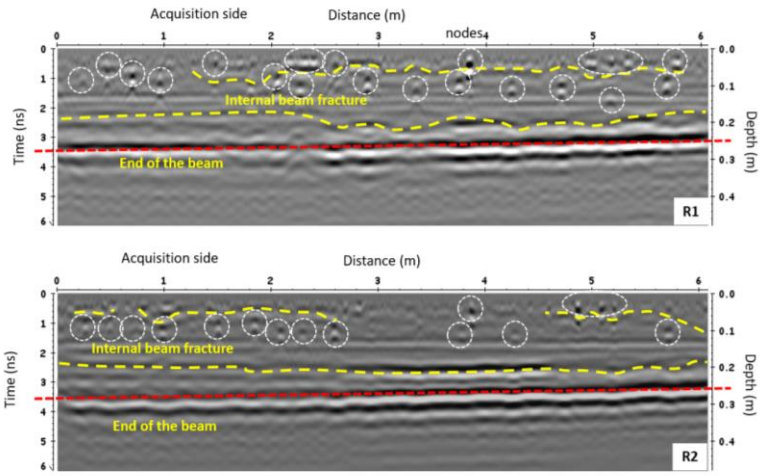

Fig. 18- The processed radar sections surveyed wooden structures (the white circles relate to the nodes indicate hyperbolic responses)

the GPR data (Fig. 18) show that: the radar signal has an excellent penetration and crosses the element investigated for all its thickness; the surface portion of the wooden structures, for a thickness varying from 0.22 to 0.25 m, is generally characterized by reflections of weak amplitude, and this testifies to

a net decrease in the density of the wood, probably related to both the activity of wood-eating insects and chemical attack; this anomaly appears to be more extensive on the extrados of the chains where the infiltration of rainwater, in the presence of significant accumulations of guano, may have generated a corrosive action resulting in breakdown of the cellular elements of the wood; the numerous reflections in the shape of hyperbole, placed at various depths indicate hardening of woody tissue

that, in size and shape, can be related to nodes, single or in groups, their number, sometimes high, determines an average density including between 3 and 5 nodes per meter, but in some elements of the apse area will reach higher values; reflections with continuous development are generated by sub-horizontal fissures almost always oriented in the direction of the grain; their width is generally close to 1 cm.

Using a point-source reflection from a buried object (white circles) to determine the 2D distribution of the EM wave velocity and the use of the relationship shown in Fig. 11 gives an accurate (qualitative) estimate of the volumetric water content (Fig. 19).

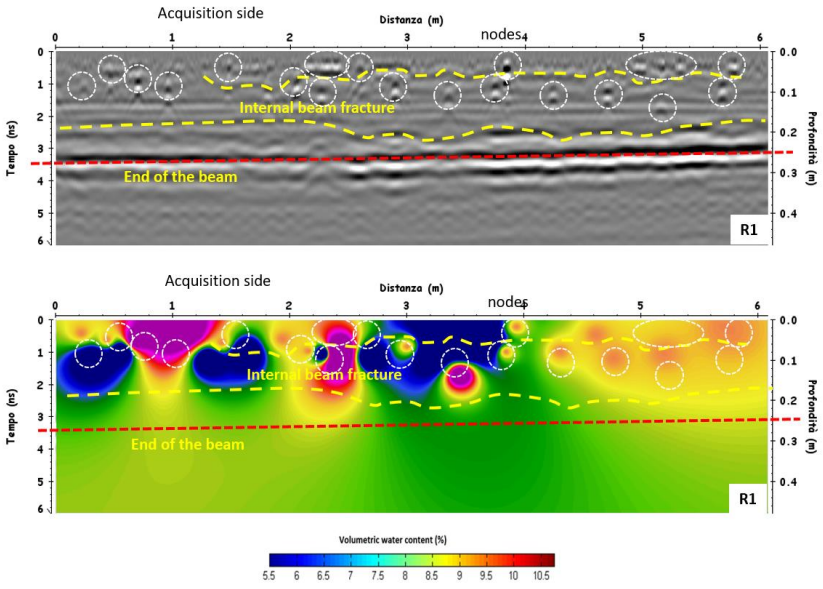

Fig. 19 - The distribution of volumetric water content

The 2D distribution of the volumetric water content of the wood varies from about 5% to 10% (Fig. 19). Water content was also measured through a direct mode using a wooden core, and results agree with those obtained using our relationship.

Conclusions

In this paper, an experimental comparison between GPR and TDR measurements to determine the dielectric permittivity of a series of wood samples was proposed. Furthermore a method to estimate the dielectric constant using the diffraction curve by GPR data was used.

Once the dielectric constant was estimated using both the GPR method and the TDR method on the same wood samples, we tried to find a relationship between the dielectric constant and the volumetric content in water. All the data obtained were entered into a graph which expresses the volumetric content values in water as a function of the dielectric constant. The data were correlated with the third degree polynomial equation that seems the best choice as we get the correlation coefficient R2 has a value of 0.837. With other types of fitting the R2 value was found to be lower. It must clearly be said that the quality of the fit appears much poorer for values of dielectric constant greater than 5. This could be due to the microscopic characteristics of the various types of woods examined. Therefore The third degree polynomial equation was used as empirical relationship between the volumetric water content and dielectric constant.

The GPR measurements on the case studied allowed the presence of various abnormalities that correspond to nodes and/or slots, making possible a rapid and accurate analysis of the electromagnetic waves velocity of propagation and thus obtaining the depth of these anomalies. Among the main obtained data, it is worth stressing the following: the surface portion of the beams, for a thickness varying from 2 to 5-6 cm, is characterized by abnormalities related to the activity of wood-eating insects and chemical attacks due to pigeon droppings; the numerous reflections in the form of hyperbole, located at various depths, indicate that hardening of woody tissue can be mapped, both in size and shape, as nodes; the continuous reflections with a sub-horizontal development are generated by fissures almost always oriented in the direction of wood fibres; in some of the trusses wooden elements of the nave has recorded the presence of cavities with dimensions of about 5 cm.

Volumetric water content analysis shows an approximately homogeneous distribution of the moisture in the analyzed woods elements.

References

Al Hagrey SA (2006) Electrical resistivity imaging of tree trunks. Near Surf Geophys 4:179–187

Balestrieri E., De Vito L., Rapuano S., Slepicka D., 2012. Estimating the uncertainty in the frequency domain characterization of digitizing waveform recorders, IEEE Trans. on Instrum. and Meas., vol.61, No.6, pp.1613-1624.

Baranski J., Suchta A. , Baranska S., Klement I., Vilkovská T., Vilkovský P., 2021. Wood Moisture-Content Measurement Accuracy of Impregnated and Nonimpregnated Wood Sensors 2021, 21, 7033. https://doi.org/10.3390/s21217033

Cataldo A., De Benedetto E., Cannazza G., 2011. Broadband reflectometry for enhanced diagnostics and monitoring applications", Springer Verlag, ISBN 978-3-642-20232-2.

Cataldo A., Cannazza G., De Benedetto E., Tarricone L., and Cipressa M., 2009. Metrological assessment of TDR performance for moisture evaluation in granular materials, Measurement, vol. 42, no. 2, pp. 254–263.

Daniels, D. J., 2004. Ground penetrating radar 2nd edition, IEE press.

EN 13183-1:2002, Moisture content of a piece of sawn timber - Part 1: Determination by oven dry method; European Committee for Standardization CEN, Brussels, Belgium, 2002.

EN 13183-3:2005, Moisture content of a piece of sawn timber - Part 3: Estimation by capacitance method; European Committee for Standardization CEN, Brussels, Belgium, 2005

Jol H., 2009. Ground Penetrating Radar: Theory and applications, Elsevier.

Giannino F., Leucci G., 2021. Electromagnetic Methods in Geophysics: Applications in GeoRadar, FDEM, TDEM, and AEM. Wiley, pp 352, ISBN: 978-1-119-77098-5

Kollmann, F., Coté, W., A., Principles of Wood Science and Technology I: Solid Wood, Springer, Berlin, 1968.

Lambot S., Slob. E. C., van den Bosch I. Stockbroeckx B.and Vanclooster M., 2004. Modeling of ground-penetrating radar for accurate characterization of subsurface electric properties. IEEE Transaction on Geoscience and Remote Sensing, 42: 2555-2568.

Leucci G., Persico R., Soldovieri F., 2007. Detection of Fracture From GPR data: the case history of the Cathedral of Otranto, Journal of Geophysics and Engineering, vol. 4, pp. 452-461.

Leucci G., 2019, Nondestructive Testing for Archaeology and Cultural Heritage: A practical guide and new perspective. Springer editore pp 217, ISBN 978-3-030-01898-6

Mai T. C., Razafindratsima S., Sbartaï Z. M., Demontoux D., Bos F. 2015. Non-destructive evaluation of moisture content of wood material at GPR frequency. Construction and Building Materials 77 (2015) 213–217

Niemz, P., Physik des Holzes und der Holzwerkstoffe, DRW-Verlag, Leinfelden-Echterdingen, 2003.

Robinson D. A., Schaap M., Jones S. B., Friedman S. P., Gardner C. M. K., 2003. Considerations for improving the accuracy of permittivity measurement using time domain reflectometry: air-

water calibration, effects of cable length, Soil Science Society of America Journal, vol. 67, pp. 62-70.

Soldovieri F., Prisco G., Persico R., 2008. Application of Microwave Tomography in Hydrogeophysics: e examples, Vadose Zone Journal, pp. 160-170.

Soldovieri F., Prisco G., Persico R., 2009. A strategy for the determination of the dielectric permittivity of a lossy soil exploiting GPR surface measurements and a cooperative target", Journal of Applied Geophysics, vol. 67, no. 4, pp. 288-295.

Topp G. C, Davis J. L., and Annan A. P., 1980. Electromagnetic determination of soil water content: measurements in coaxial transmission lines, Water Resources Research, vol. 16, no. 3, pp. 574-582.